Journal of Power Sources 198 (2012) 66–75

Contents lists available at SciVerse ScienceDirect

Journal of Power Sources

journal homepage: www.elsevier.com/locate/jpowsour

Characterization of sulfated-zirconia/Nafion® composite membranes for proton exchange membrane fuel cells

Guinevere A. Giffin[a], Matteo Piga[a], Sandra Lavina[a], Maria Assunta Navarra[b], Alessandra D'Epifanio[c], Bruno Scrosati[b,*], Vito Di Noto[a,*]

[a] Dipartimento di Scienze Chimiche, Universitàdi Padova, Via Marzolo 1, I-35131 Padova (Pd), Italy
[b] Dipartimento di Chimica, Universitàdegli Studi di Roma "La Sapienza", Piazzale Aldo Moro 5, 00185 Roma, Italy
[c] Department of Chemical Science and Technology, University of Rome "Tor Vergata", Via della Ricerca Scientifica, 1, 00133 Roma, Italy

ARTICLE INFO

Article history:
Received 17 August 2011
Received in revised form
26 September 2011
Accepted 27 September 2011
Available online 4 October 2011

Keywords:
Hybrid membrane
Nafion
Sulphated-zirconia filler
Broadband electric spectroscopy
Proton conduction mechanism
Molecular relaxations

ABSTRACT

An interesting new material based on a Nafion® membrane doped with a sulfated-zirconia filler is presented. This filler is unique in that the filler itself can contribute to the proton conductivity due to the presence of acidic functionalities on the surface of the filler. The presence of the filler in the membrane results in the deprotonation of Nafion®'s acid moieties as indicated by the absence of the acid mode at 1475 cm^{-1} in the FTIR spectrum. Spectra from DSC, DMA and broadband electric spectroscopy (BES) show the presence of several molecular transitions, two of which are detected in the BES permittivity profiles. The membrane exhibits a reasonably high conductivity (3×10^{-3} S cm^{-1} at 120 °C) even in completely dry conditions, which makes it a promising material for an anhydrous fuel cell. The conductivity behaviour exhibits a mix of Arrhenius and VTF behaviours and is closely tied to the dielectric relaxations.

1. Introduction

Perfluorinated polymers such as Dupont's™ Nafion®[1] have been the focus of research for many years for application in proton exchange membrane fuel cells. However, at elevated temperatures, i.e. above 100 °C, pristine Nafion® suffers from reduced conductivities due to a loss of water from the system [1,2]. This particular downfall of Nafion® is problematic because most current electrocatalysts have enhanced reaction kinetics and are less susceptible to poisoning at these operating temperatures [2,3]. Elevated temperatures also would obviate the need for water management systems and simplify thermal management [4,5]. One approach to overcome the problems associated with pristine Nafion® is to introduce a filler into the membrane to improve the thermal, mechanical and electrical properties of the membrane [1,4]. Generally these fillers are located at the interfaces between the hydrophilic and hydrophobic domains of the membrane matrix and help establish percolation pathways for proton conduction. Many different types of fillers, including inorganic, ionic liquids and organic–inorganic fillers, have been used in the production of hybrid membranes [1,6–12]. Some of these fillers, such as simple inorganic metal oxides or "core–shell" nanofillers, participate in the proton conduction mechanism but do not contribute to the charge carrier concentration in the system [7,13–17]. Recently, a novel sulfate-functionalized zirconia-based (S-ZrO_2) filler has been investigated as a proton conductor [18–23]. This filler, like heteropolyacids [24–26], functionalized zeolites [27,28], sulfonated-POSS [29,30] and proton-conducting ionic liquids [5,8,10,11], is unique because the acidic moieties on the zirconia surface allow it to contribute directly to modulation of the "free" proton density, which influences the percolation pathway in the bulk membranes. Fuel cell tests using Nafion® composite membranes containing 5% S-ZrO_2 showed a general improvement in the power density and the ohmic resistance when compared to a Nafion®-containing cell [18]. The enhanced performance at high temperatures and low relative humidities [18,19,31], i.e. 20% relative humidity, makes these materials particularly interesting for application in medium-high temperature fuel cells.

In previous studies some of the thermal properties and the overall conductivity of 5% S-ZrO_2/Nafion® composite membranes have been investigated along with the fuel cell performance

* Corresponding authors. Tel.: +39 049 827 5229; fax: +39 049 827 5229.
E-mail address: vito.dinoto@unipd.it (V. Di Noto).

[1] The DuPont Oval Logo, DuPont™, The miracles of science™ and all products denoted with a ™ and ® are trademarks or registered trademarks of DuPont or its affiliates.

0378-7753/$ – see front matter © 2011 Elsevier B.V. All rights reserved.
doi:10.1016/j.jpowsour.2011.09.093

[18,19,22,31], but an in-depth study of the mechanical and electric properties has not been reported. In this study, composite membranes containing 5% of the S-ZrO_2 filler are characterized with differential scanning calorimetry (DSC), dynamic mechanical analysis (DMA), Fourier transform infrared spectroscopy (FTIR) and broadband electric spectroscopy (BES) to investigate the mechanical and electrical properties of the membrane and to relate those properties to the membranes' structure. The membranes were studied in both humidified and non-humidified conditions to examine the difference in the behaviour and interactions in the presence of water.

2. Experimental

2.1. Sample preparation

Sulfated-zirconia, which has a tetragonal crystalline structure, and the composite S-ZrO_2/Nafion® membranes were prepared as previously described [19,22,31]. The "dry" samples were obtained by drying the polymers for 48 h under vacuum at 120 °C. The "wet" samples were obtained by autoclaving the material at 120 °C for 35 min at 100% relative humidity and then immersing it in milli-Q water overnight at room temperature.

2.2. Instruments and methods

Thermal characterization was performed with TG and DSC. TG analyses were performed with a High Resolution TGA 2950 (TA Instruments) thermobalance working under a N_2 flux of 100 $cm^3\,min^{-1}$ and with a resolution of 1 μg. A 2920 differential scanning calorimeter (TA Instruments) equipped with a liquid nitrogen cooling system operating under a helium flux of 30 $cm^3\,min^{-1}$ with a heating rate of 3 °C min^{-1} in the temperature range from −150 to 350 °C was used to probe the thermal phase transitions. Samples of approximately 4 mg were hermetically sealed in an aluminum pan.

DMA measurements were made with a TA Instruments DMA Q800 equipped with film/fiber tension clamp for testing films in the tension mode. Spectra were collected by applying a sinusoidal deformation of amplitude 4 μm at 1 Hz in 4 °C intervals over a thermal range from −150 to 220 °C. A 25 mm × 6 mm × 0.2 mm rectangular sample was subjected to a pre-loading force of 0.05 N. The viscoelastic behaviour of the samples was quantified in terms of elastic modulus (E'), loss modulus (E'') and loss factor ($\tan\delta$).

FTIR spectra were collected using a Nicolet FTIR Nexus spectrometer with a resolution of 4 cm^{-1}. The spectra of the membranes were obtained in ATR mode with a Perkin-Elmer Frustrated Multiple Internal Reflections 186-0174 accessory.

Electric spectra were measured with BES in the frequency range from 10 mHz to 10 MHz using a Novocontrol Alpha analyzer over the temperature range from −155 to 155 °C. The temperature was controlled using a homemade cryostat operating with an N_2 gas jet heating and cooling system. Temperature was measured with accuracy greater than ±0.05 °C. Membranes were sandwiched between two circular platinum electrodes inside a closed cylindrical homemade teflon cell. The cell was closed to avoid water loss during the measurement of wet samples and water adsorption before the measurement of the dry samples. Weighing the closed cell before and after measurements indicated that there was no water loss during the wet measurements. The geometrical cell constant was determined by measuring the electrode–electrolyte contact surface and the distance between electrodes with a micrometer. Corrections for thermal expansion of the cell were not used.

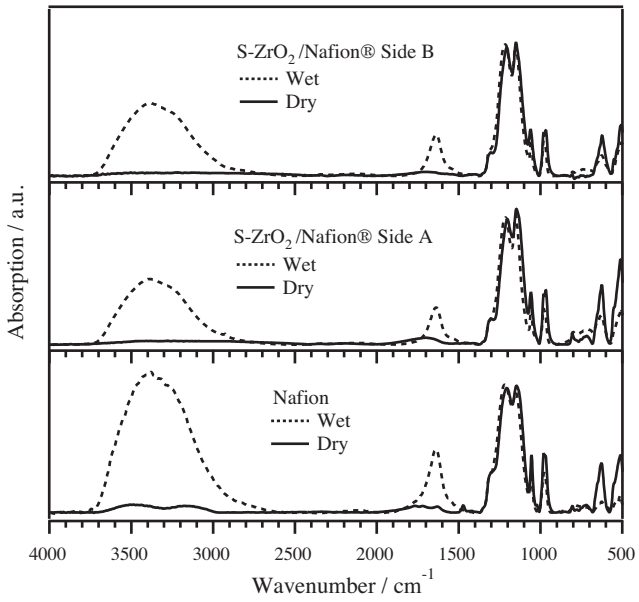

Fig. 1. FTIR ATR spectra of the S-ZrO_2/Nafion® composite membrane and pristine Nafion®. Side A refers to the top side of the membrane after the casting process, while side B refers to the bottom side of the membrane.

3. Results and discussion

3.1. FT-IR spectroscopy

The infrared spectra of the hybrid membrane, which are shown in Fig. 1, exhibit similar spectral characteristics to that of pristine Nafion®. Previous work has shown that the principle features of the S-ZrO_2 spectra are the sulfate bands between approximately 1400 and 1000 cm^{-1} [20,32]. In the spectrum of the composite membrane these bands are indistinguishable from the Nafion® bands. This is unsurprising given that the filler and Nafion® contain some similar functionality, the filler comprises only 5 wt% of the membrane and the CF_2 modes of Nafion occur in this spectra region [16]. Both sides of the membrane show spectra that are almost identical. This indicates that the membranes are homogeneous. Side A refers to the top side of the membrane after the casting process, while side B refers to the bottom side of the membrane. The small spectral shifts occurring in the CF_2 region with membrane hydration mirror those of pristine Nafion® and are likely attributed to conformational changes within some fraction of the host polymer [8,15,33]. The effect of the filler is much more evident in the water stretching region centred at ca. 3400 cm^{-1}. The intensity of this broad band in pristine Nafion® is approximately double that found in the hybrid membrane. This trend is in good agreement with the water uptake values determined by TG, which show an uptake of 25 and 15 wt% for pristine Nafion® and the composite membranes, respectively.

The most significant difference in the FTIR spectra of the composite membrane and pristine Nafion® is found in the Nafion® acid mode region found above the strong CF and CC stretching modes. This spectral region is shown in Fig. 2. In dry Nafion®, a weak band can be found at approximately 1475 cm^{-1} that has been attributed to a sulfonate group with a covalently bound (undissociated) proton [16]. This band disappears upon hydration of the pristine Nafion® as the proton dissociates forming the sulfonate anion and a proton associated with the water present in the system. Unlike the spectrum of pristine Nafion®, this band is not present in the spectrum of composite membrane indicating that the protons are dissociated from Nafion®'s pendant side chains even in completely dry conditions. This result is different from that found in

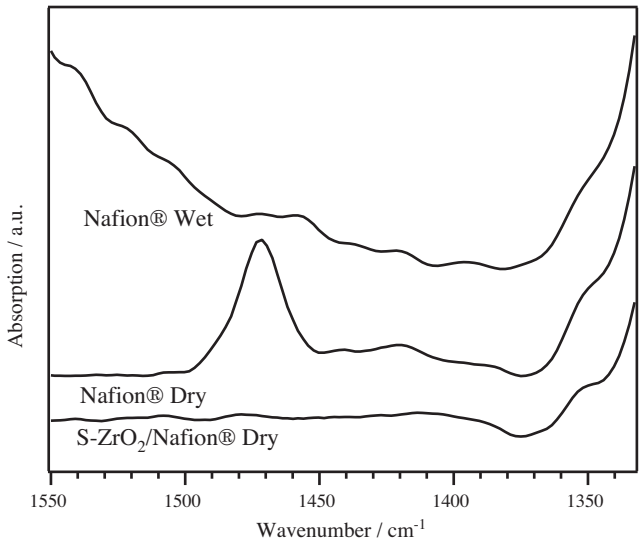

Fig. 2. FTIR ATR spectra of the S-ZrO_2/Nafion® composite membrane and pristine Nafion® in the acid mode region.

some other composite systems. For example, in Nafion® composite membranes doped with "core–shell" nanofiller, the acid band of Nafion® remains in the presence of the nanofiller indicating that the proton is still covalently bonded to the pendant side chain [16]. The fact that there are no undissociated protons on the Nafion® side chains in the composite membrane has important implications for its structure, suggesting that the filler in the composite increases the number of charge carriers present in the dehydrated system as compared to pristine Nafion®.

Previous studies [21,34,35] on this filler have indicated that the presence of sulfates on the zirconia surface allows S-ZrO_2 to function as both a Lewis and Bronstead acid. In the absence of water, the protons dissociated from the Nafion® side chains could be associated with a bidentate sulfate (Fig. 3). This hypothesized structural model could result in the sulfate becoming monodentate, which would allow it to rotate towards an adjacent Lewis acid site. In

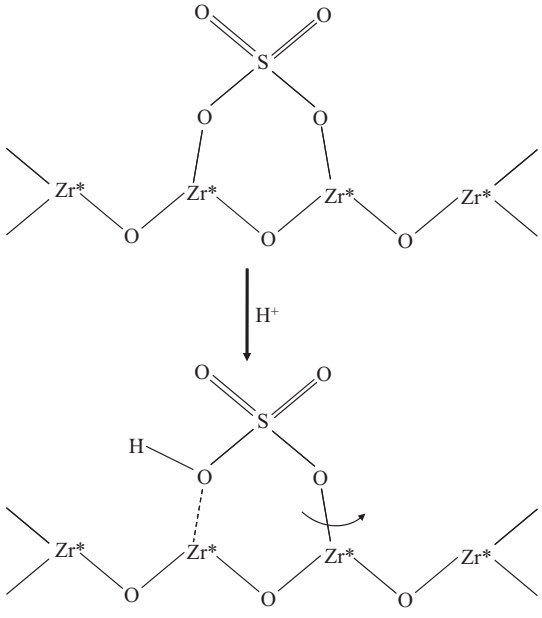

Fig. 3. Hypothesized structural model for the interaction of protons with the S-ZrO_2 surface. The * indicates a Lewis acid site.

such a way, the protons can moved along the surface of the filler. In the presence of water, protons can be moved along the surface of the filler by the exchange of Lewis and Bronstead acid sites [21,34].

3.2. DSC, DMA and BES analyses

Combining the DSC curves with the tan δ profiles from DMA and BES reveal the presence of one γ, two β and three α relaxation events in both the S-ZrO_2/Nafion® composite membrane and pristine Nafion® [36], as shown in Fig. 4 for the dry membrane and in Fig. 5 for the wet membrane. While not all of these transitions are clearly visible in all of the curves of Figs. 4 and 5, the combination of the three data sets allows all of the events to be readily identified. At very low temperatures, a γ transition is identified at approximately −115 °C and is associated with local fluctuations of CF_2 units along the main Nafion® fluorocarbon chain [37–39]. This peak is stronger and occurs at slightly higher temperatures in the wet spectra than in the dry spectra. Two β relaxations associated with the polyether side chains can be found between −84 and −20 °C for the S-ZrO_2/Nafion® composite membrane. The higher temperature event, β_1, can be attributed to conformational transitions of the ether group bound to the backbone end of the side chain, while the lower temperature event, β_2, can be attributed to conformational transitions of the ether group bound to the sulfonate end of the side chain [36]. The separation between the γ and the β transitions is more clearly visible in wet membranes than in the dry membranes, possibility due to the plasticizing effect of water. There are three alpha transitions above 0 °C: α_1, α_2 and α_{pc}. α_1 and α_2, the lower temperature transitions in this region, are associated with conformational transitions of the main perfluorocarbon chain, while α_{pc}, found at temperatures above 100 °C, is associated with the long-range movement of the fluorocarbon domains and side chains due to weakening of electrostatic interactions within the hydrophilic domains [8,16,40]. In both the wet and dry hybrid membrane an increase above 40 °C is seen in the DMA tan δ spectra. The maximum value of this increase occurs at the same position as the peak at approximately 100 °C corresponding to the α_{pc} mechanical transition in pristine Nafion. The α_{pc} mechanical transition occurs due to the absorbance of mechanical energy associated with the weakening of the polar interactions between domains. It is likely that the increase in the hybrid membrane spectra is the start of the α_{pc} mechanical transition, but the weakening of the interactions leads to the total mechanical failure of the hybrid membrane at approximately 100 °C. In the fully hydrated hybrid system, the α_1 and α_2 transitions are found to be closer together in temperature, more well-resolved and correspond to an increased intensity of the γ transition than in the dry hybrid membrane. As these transitions depend on the conformation of the main polymer chain, this behaviour could indicate an increased crystallinity in the hydrophobic domains of the host matrix. Crystallinity in the hydrophobic domains could result from decreased interaction strength of the side chains due to the plasticization by water and result in an increased distribution of the side chain configurations. This is supported by a splitting of the β transitions particularly in the BES tan δ spectra.

There are other thermal and mechanical properties worth mentioning in addition to those already discussed. The storage modulus of the dry composite membrane (79 MPa at 80 °C) is lower than that of pristine Nafion (205 MPa at 80 °C) [36] and other ZrO_2 composite membranes [7]. Nafion undergoes an irreversible elongation at slightly higher temperatures than the composite membrane (Figs. 4b and 5b). The composite membrane in fully hydrated conditions has severely reduced mechanical properties throughout the entire temperature range, probably due to plasticization by water.

Some of the dielectric relaxations discussed with respect to Figs. 4 and 5 for the composite membrane can be found, along with

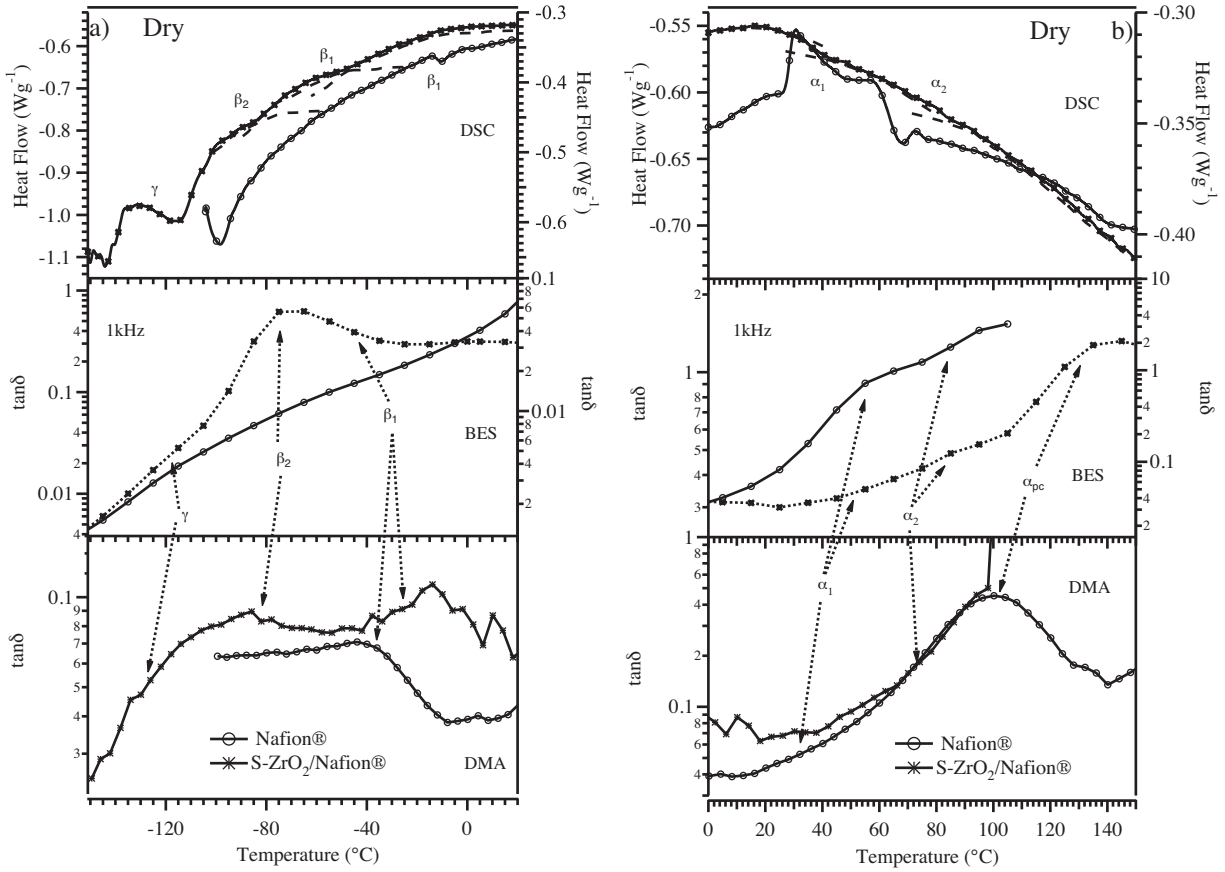

Fig. 4. Profiles of heat flow from DSC and tan δ from DMA and BES for dry S-ZrO_2/Nafion® and pristine Nafion®. The data for Nafion® reported by Di Noto et al. are included for the sake of comparison [36]. Temperature ranges (a) from −150 to 20 °C and (b) from 0 to 150 °C.

polarization events, in the imaginary component of the permittivity, ε'', shown as a function of both frequency and temperature. The ε'' and the σ' surfaces can be seen in Fig. 6 for the dehydrated membrane. The most prominent feature of the ε'' surface is the strong peak that starts at low frequency at lower temperature that shifts to higher frequency with increasing temperature. This peak, denoted as σ_0 in Fig. 6, is due to the electrode polarization phenomenon and corresponds to the beginning of a plateau in the real component of the conductivity σ' that is associated with the bulk or DC conductivity [41]. Two dielectric relaxations can be seen on the low permittivity side of the σ_0 peak in the ε'' surface and correspond to an increase in σ'. The relaxation starting at higher frequency corresponds to the β_2 transition, while the one at low frequency corresponds to β_1. Both relaxations move to higher frequency with increasing temperature and by 0 °C both events have moved out of the experimental frequency range. Two broad peaks can be seen on the low frequency side of σ_0 in the ε'' surface. Labelled σ_1 and σ_2 in Fig. 6, these two peaks correspond to inflection points in σ' and are attributed to interfacial polarizations associated with charge accumulation along the interface of domains with different permittivities [16]. It should be noted that the α relaxations cannot be distinguished in the ε'' surface. These relaxations are covered by interfacial polarizations σ_1 and σ_2 that have permittivity values larger than any of the dielectric relaxations. The α transitions can be seen clearly at temperatures above 0 °C in the BES tan δ spectra in Figs. 4 and 5 because the polarizations, which causes an increase in both the real and imaginary parts of the permittivity, are typically suppressed in tan δ [36,42,43].

Similar events can be seen in the ε'' and the σ' surfaces of the fully hydrated membrane in Fig. 7, where two dielectric relaxations, one electrode polarization and two interfacial polarizations are present. The presence of water above its melting point changes both surfaces as indicated by a step increase in the electrode polarization and is associated with an increase in σ' by three orders of magnitude. Below 0 °C, both surfaces resemble that of the dry membrane. In this temperature realm, water does not contribute significantly to the conduction mechanism and the strength of the interactions involving water likely remains fairly constant. These observations are in agreement with previously reported results [36].

The conductivity values associated with the various polarization events, dielectric strengths and the characteristic relaxation times are obtained by fitting the experimental ε'' and ε' profiles with a general empirical equation [7,42,44]:

$$\varepsilon^*(\omega) = i\left(\frac{\sigma(T)}{\varepsilon_0\omega}\right)^{N(T)} + \sum_{k=0}^{2}\frac{\sigma_k(i\omega\tau_k)^{\gamma_k}}{i\omega[1+(i\omega\tau_k)^{\gamma_k}]} + \sum_{j=1}^{2}\frac{\Delta\varepsilon_j}{[1+(i\omega\tau_j)^{\alpha_j}]^{\beta_j}} + \varepsilon_\infty \quad (1)$$

where $\varepsilon^*(\omega) = \varepsilon'(\omega) - i\varepsilon''(\omega)$. In this equation, the first term describes the conductivity of the material at frequencies lower than those experimentally measured, while ε_∞ accounts for the permittivity of the material at infinite frequency. The second term accounts for the polarization phenomena, where $k = 0$ for the electrode polarization and $k = 1$ or 2 for the interfacial polarizations. The variables σ_k and τ_k are the conductivity and relaxation time associated with the kth polarization event, while γ_k is a shape parameter that describes the broadening and asymmetry of the kth

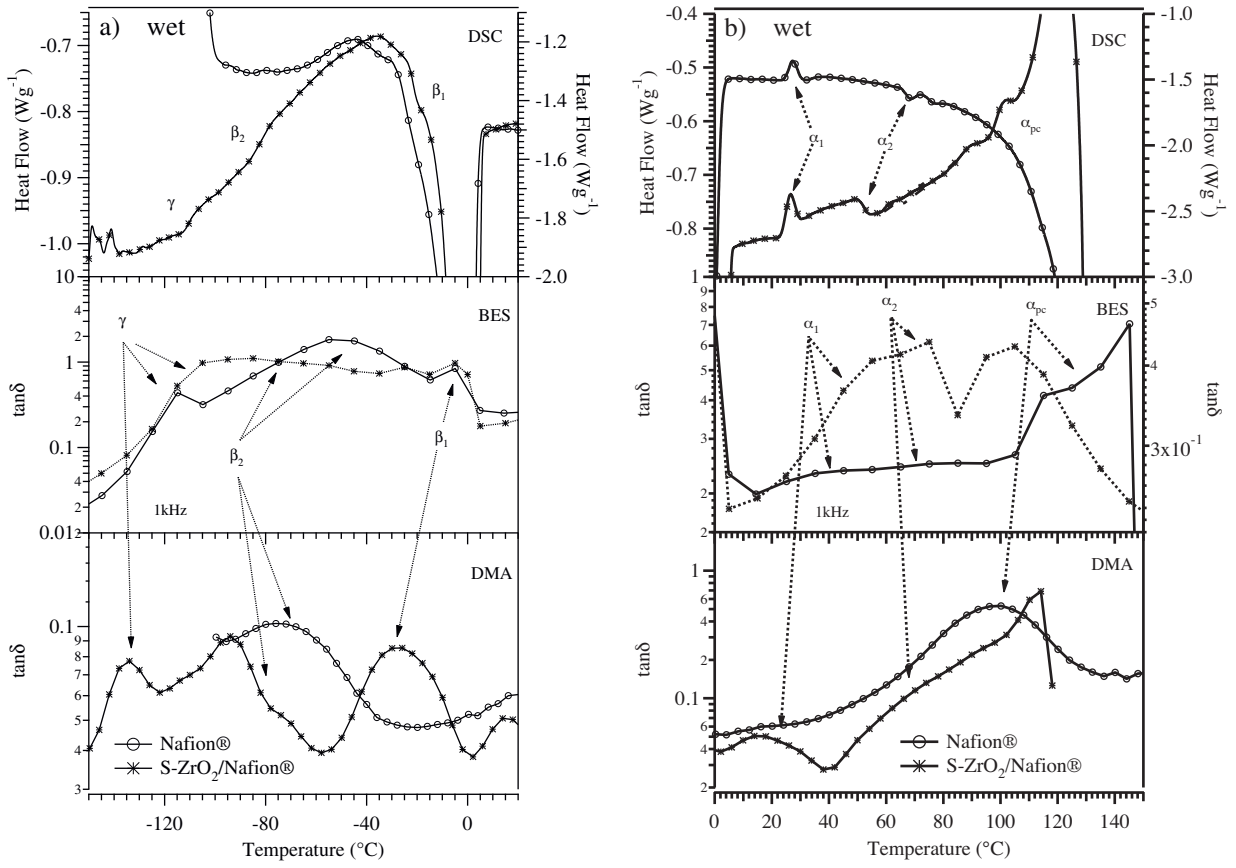

Fig. 5. Profiles of heat flow from DSC and tan δ from DMA and BES for wet S-ZrO_2/Nafion® and pristine Nafion®. The data for Nafion® reported by Di Noto et al. are included for the sake of comparison [36]. Temperature range (a) from −150 to 20 °C and (b) from 0 to 150 °C. In the cases where there are both left and right axes, the left corresponds to the hybrid membrane and the right corresponds to pristine Nafion®.

peak. The third term expresses the dielectric relaxation through a Havriliak–Negami relationship [42], where $\omega = 2\pi f$ is the angular frequency of the electric field, τ_j is the relation time of the jth event that has an intensity $\Delta\varepsilon_j$, and α_j and β_j are shape parameters that account for the symmetric and asymmetric broadening of the jth peak.

An example of the fit of ε'' and ε' profiles of the S-ZrO_2/Nafion® hybrid membrane at −25 °C can be seen in Fig. 8. In this temperature region, two conductivity terms, σ_0 and σ_1, and one dielectric term, β_1, are revealed. From this point as temperature increases, the dielectric term moves out of the experimental range on the high frequency end of the spectra. At this temperature, only the start of the peak associated with the interfacial polarization σ_1 is included in this frequency range, but an increase in both the ε'' and ε' profiles at low frequency indicates that it is necessary to achieve a good fit of the data. In the ε' spectrum, the ε_∞ term is necessary to fit the data at very high frequency to correct for the inherent permittivity of the material. A good fit of the data is achieved when both the real and imaginary components of the permittivity, along with σ'', σ', and tan δ are reasonably well matched simultaneously.

The conductivity values associated with the electrode polarization σ_0 and the interfacial polarizations σ_1 and σ_2 obtained by fitting the permittivity data with Eq. (1) are shown as a function of reciprocal temperature in Fig. 9. The conductivity behaviour of the composite membranes is complex and closely bound to the relaxations discussed in Figs. 4 and 5. The complex nature is clearly evident from the presence of several distinct regions in the conductivity curves. In the dry composite membrane, the conductivity profile σ_0 can be divided into four temperature regions (Fig. 9, part a). At very low temperatures, there are two regions with very different activation energies that follow Arrhenius behaviour. Arrhenius behaviour in this very low temperature, and therefore low thermal energy region, indicates that in these conditions the conductivity follows a Grotthus-like "hopping" process [45]. The breakpoint between the temperature regions I and II corresponds to the γ relaxation found at −115 °C. The lower temperature region (I) has an activation energy of 9.3 ± 0.9 kJ mol^{-1}, while the higher temperature region (II) has an activation energy of 51 ± 4 kJ mol^{-1}. This higher activation energy indicates that the γ transition actually hinders the proton hopping process and the long range conductivity. The γ transition, which liberates some of the movement of the main perfluorocarbon chain perpendicular to the chain axis, could actually result in a more tortuous path between hopping sites and the elevated activation energy.

The next significant change in behaviour of σ_0 is found as a step increase in the conductivity between −65 and −75 °C, which corresponds to the β_2 transition, and results in a change from Arrhenius to Vogel–Tammann–Fulcher (VTF) behaviour. This trend indicates that the mechanism of long range conduction shifts from a Grotthus-like 'hopping' conduction process to a conductivity facilitated by the fluctuations of the CF_2 units of the membrane [45]. The VTF fit of the data in region III between −65 and 75 °C results in a pseudo-activation energy of 10 ± 1 kJ mol^{-1} and a T_0 of −145 °C. This T_0 is reasonably close in temperature to the γ transition, indicating that in this temperature realm the long range conduction mechanism is facilitated by the motion of the polymer backbone perpendicular to the chain axis. The beginning of this behaviour at a temperature corresponding to the β_2 transition indicates that although main chain facilitates that movement, the β_2 transition is responsible for the change from Arrhenius to VTF behaviour

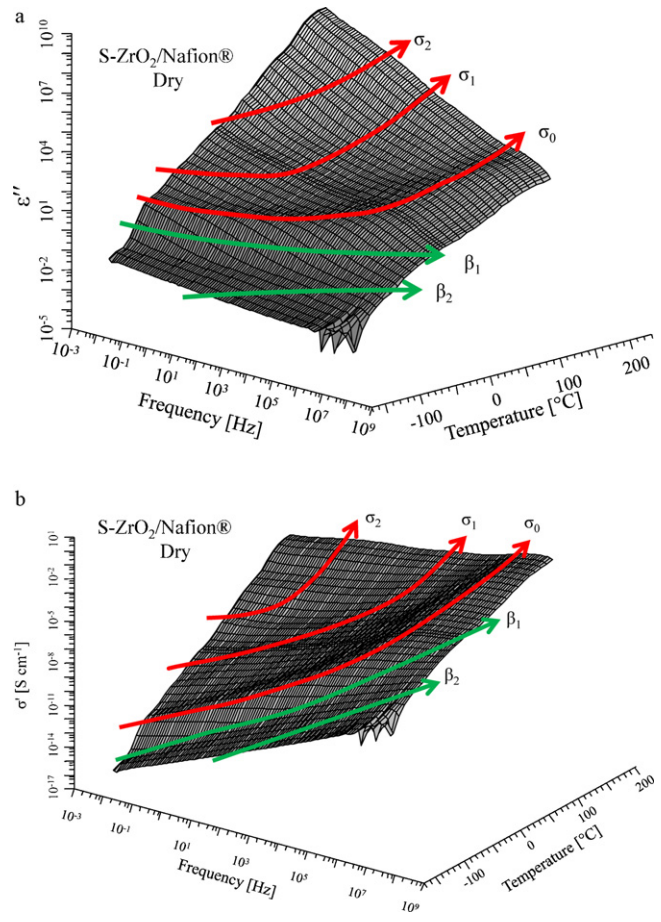

Fig. 6. 3D plot of the imaginary component of the permittivity and the real component of the conductivity as a function of temperature and frequency for the dry S-ZrO_2/Nafion® membrane.

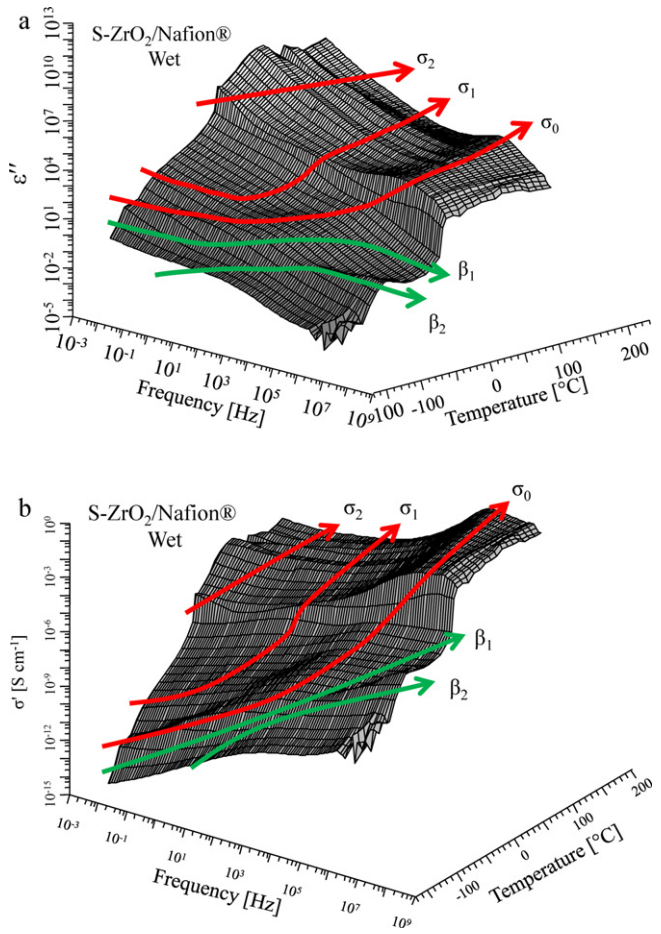

Fig. 7. 3D plot of the imaginary component of the permittivity and the real component of the conductivity as a function of temperature and frequency for the wet S-ZrO_2/Nafion® membrane.

possibly because as the side chains become more mobile, they are more susceptible to the motion of the main chain.

At temperatures above 75 °C (region IV), the conductivity follows VTF behaviour with a pseudo-activation energy of 1.6 ± 0.7 kJ mol^{-1} and a T_0 of 33 °C. This T_0 corresponds to the temperature of the α_1 transition. In this temperature region, the long range conductivity is mediated by the segmental motion of the main fluorocarbon chains in the PTFE hydrophobic domains of Nafion®. The additional mobility of the polymer backbone, which assists in the charge motion, is responsible for the large decrease in the pseudo-activation energy seen between regions III and IV.

In a completely dehydrated state, the conductivity σ_0 of the composite membrane is between 4 and 8 orders of magnitude higher than that of pristine Nafion® between 105 and 15 °C [36]. The pseudo-activation energy for pure Nafion in this temperature range is 35 ± 8 kJ mol^{-1} [36], which is significantly higher than either of those reported for the composite membrane above. The presence of the filler in the membrane significantly improves the conductivity in anhydrous conditions by creating additional percolation pathways for charge conduction and increasing the number of charge carriers in the system. This greatly improved conductivity makes the composite membrane a promising material for application in an anhydrous fuel cell.

The conductivity σ_0 of the composite membrane in a fully hydrated state bears resemblance to that of the composite membrane in the dry state below the melting point of water. However, unlike in the dry system, there is no membrane mediation of the conductivity in this region as revealed by the absence of VTF behaviour. The presence of solid water, which solvates the end groups in the hydrophilic domains of the membrane, results in a decoupling of the motion of the Nafion® side chains and the perfluorinated backbone. This conductivity region can be divided into four temperature realms, where the breakpoint temperature between each region corresponds to one of the three low temperature relaxation modes, γ, β_2, and β_1. The activation energies for these temperature realms are found to be 24 ± 3 (region I), 62 ± 1 (region II), 21.6 ± 0.6 (region III) and 51 ± 5 (region IV) kJ mol^{-1} moving from low to high temperature. As in the dry membrane, a significant increase in the activation energy is seen after the γ relaxation. The β_2 relaxation at approximately −85 °C provides more freedom of movement in the side chains which seems to making hopping sites more accessible resulting in a decrease in the activation energy. However at the β_1 relaxation, the activation energy increases again. After the β_1 relaxation, it is possible that the immobile ice crystals found in the hydrophilic domains of the membrane provides a large steric hindrance to proton hopping in the presence of the highly mobile side chains, resulting in a poor pathway for long range conductivity.

Below the melting point of water, the conductivity σ_0 of Nafion® is between one and two orders of magnitude lower than that of the composite membrane. In addition, pristine Nafion® has activation energies of 38 ± 1, 31 ± 1 and 60 ± 10 kJ mol^{-1} in regions II, III and IV, respectively. In regions III and IV, these activation energies are higher than those in the same regions for the composite membrane. As in the dehydrated membrane the presence of the filler creates percolation pathways for charge conduction and increases

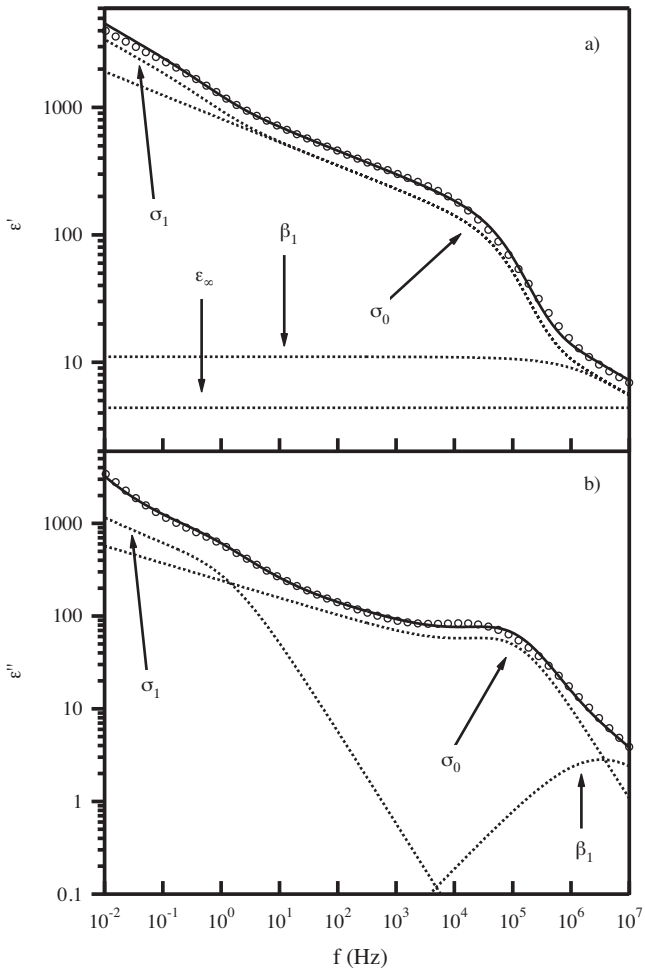

Fig. 8. Real (a) and imaginary (b) parts of the permittivity of the dry S-ZrO_2/Nafion® membrane at −25 °C with the electrical polarization and dielectric terms from Eq. (1) using two polarizations, one dielectric relaxation and the permittivity at infinite frequency. The circles represent the original data and the dark line represents the overall fit.

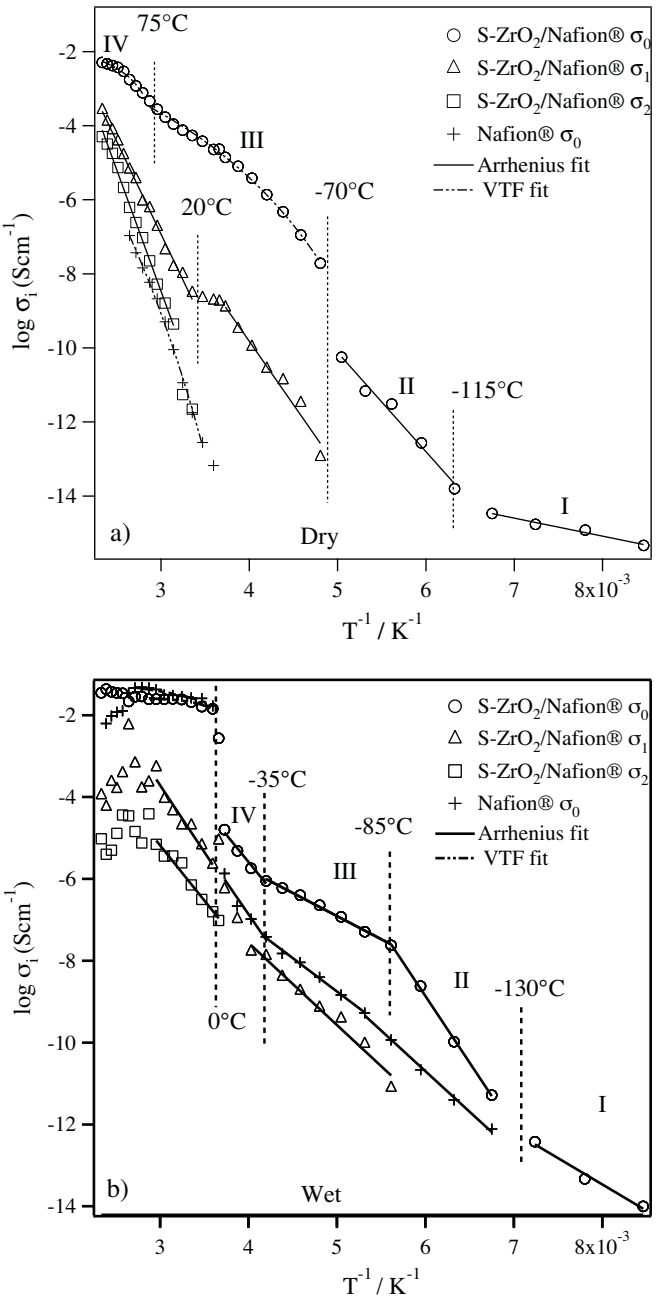

Fig. 9. Log of conductivity as a function of reciprocal temperature in (a) dry and (b) wet conditions. The conductivity data for dry Nafion® reported by Di Noto et al. are included for the sake of comparison [36].

the number of charge carriers in the system. However, in region II where the thermal energy in the system is very low, the presence of the filler surrounded by crystallized water in the hydrophilic domains combined with the movement of the Nafion main perfluorocarbon chain perpendicular to the chain axis due to the γ transition results in a poor conducting percolation pathway and a higher activation energy in the composite membrane.

Above the melting point of water, the trend in the conductivity σ_0 follows VTF behaviour with a very low activation energy, 0.2 ± 0.1 kJ mol^{-1} with a T_0 of −20 °C. This T_0 value corresponds to the melting of water. In the presence of liquid water, it is likely that the pathway for long range conduction is facilitated by water and by the motion of the polymer backbone and side chains. Unlike in the presence of solid water, the presence of VTF behaviour and a T_0 value corresponding to the β_1 transition suggests that there is coupling between the motion of the backbone and the side chain above 0 °C. Above 45 °C, the conductivity data of the composite membrane begin to show significant scattering. This is most likely due to the effect of the hydrated filler as indicated by the BES spectra of the pure filler. The BES tan δ spectra at three different frequencies and the log of the conductivity, both as a function of temperature are shown in Fig. 10. The tan δ spectra of the filler as a function of temperature reach a maximum between 25 and 40 °C that is independent of frequency and corresponds to a decrease in the conductivity. This transition could possibility correspond to an acid-base type reaction facilitated by water within the filler as indicated by the DSC result. This behaviour of the filler is reflected in the conductivity data of the membrane, making a good fit of the data in this higher temperature region difficult.

Above the melting point of water, the conductivity σ_0 of Nafion® is equal to or slightly higher than that of the composite membrane [36]. In addition, the pseudo-activation energies are also similar. For Nafion®, the pseudo-activation energy is 0.5 ± 0.2 kJ mol^{-1}. In both membranes, in this temperature realm the conduction process is facilitated by water, so it is unsurprising that there is little difference in the conductivity values. Water uptake measurements by TG indicated that pristine Nafion® contained almost two times the amount of water as the composite membrane. In the presence of an excess of water, as is likely the case in this fully hydrated

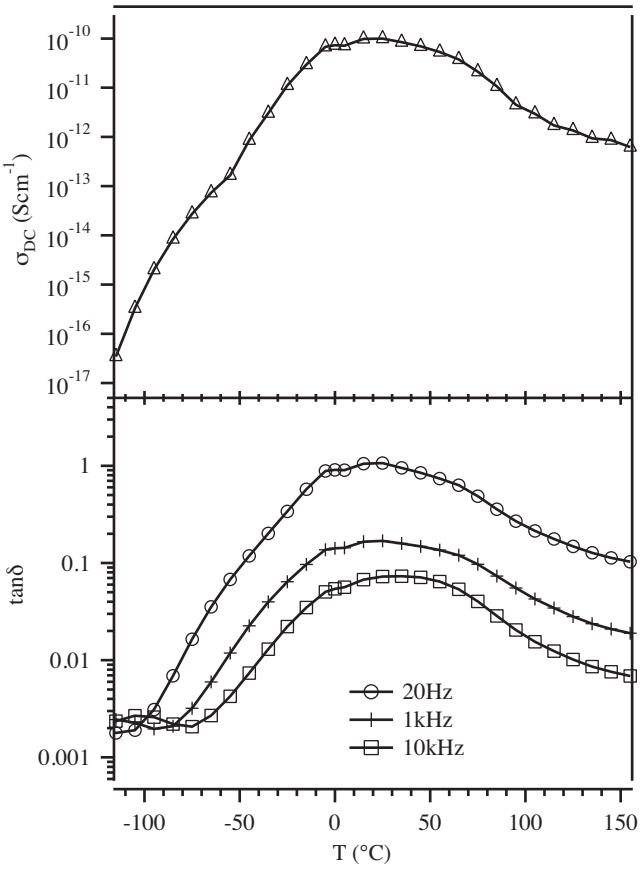

Fig. 10. BES tan δ spectra at three different frequencies and the log of the conductivity of the filler as a function of temperature.

membrane, the acid sites on the filler are likely occupied by water molecules, inhibiting the contribution of the filler itself to the conduction mechanism. This could be another factor in why this is the only region where the conductivity of the composite membrane is not higher than that of Nafion®.

It is possible to determine the mean distance of proton migration $\langle r \rangle$ between two different sites associated with the bulk conductivity using the Nerst–Einstein (2) and the Einstein–Smoluchowski (3) equations [46,47]:

$$D_{H^+} = \frac{\sigma_{dc} RT}{n_{H^+} F^2} \tag{2}$$

$$\langle r \rangle = \sqrt{6 D_{H^+} \tau_0} = \sqrt{\frac{6 \sigma_0 \tau_0 RT}{n_{H^+} F^2}} \tag{3}$$

where n_{H^+} is the charge carrier concentration, R is the universal gas constant, T is the temperature in Kelvin and F is the Faraday constant. τ_0 is the relaxation time for the conductivity σ_0. The charge carrier concentration n_{H^+} is obtained from the ionic exchange capacity [22]. The density of Nafion [48], assuming it is almost the same as the composite membrane that contains only 5% of filler, is equal to 1.65 g cm^{-3}. The values of $\langle r \rangle$ in the dry membrane, shown in Fig. 11, exhibit an exponential increase with decreasing reciprocal temperature up to a distance of 12 nm at the highest temperatures. The steeper increase and $\langle r \rangle$ values greater than 2 nm begin at temperatures corresponding to the α_1 relaxation. In the wet composite membrane and in Nafion, there is a large step increase in the average hopping distance at the melting point of water. Above 0 °C, the values of $\langle r \rangle$ are essentially the same for both membranes, increase sharply and range between 30 and 100 nm. The relatively high values of $\langle r \rangle$ are due to the inclusion of the

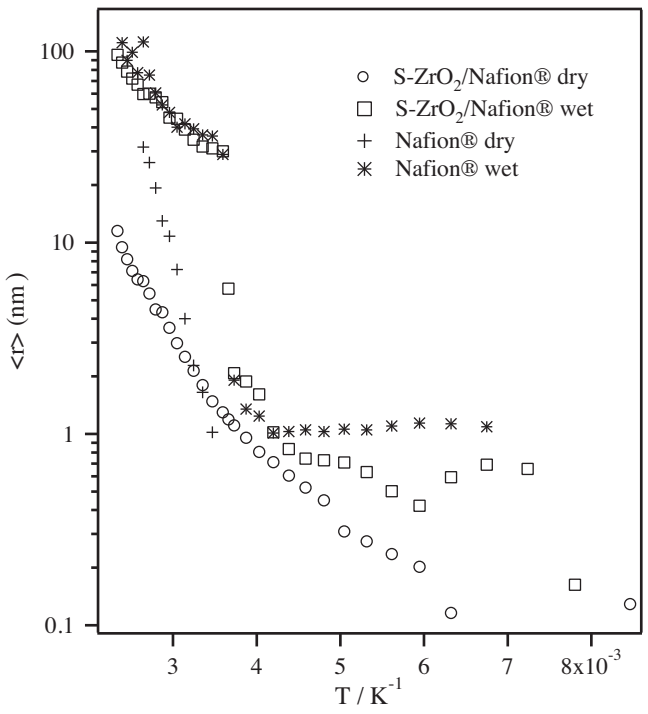

Fig. 11. Mean distance of proton migration $\langle r \rangle$ between two sites associated with the bulk conductivity in dry and wet conditions.

"bulk" conductivity in Eq. (3). Consequently, r is reported as a mean value of the proton migration distance inside polar hydrophilic domains (intra-cluster migration) and between different ionic clusters (inter-cluster migration). In this temperature realm, the proton migration is greatly influenced by the presence of water, which also accounts for the large distances calculated. Below 0 °C, the $\langle r \rangle$ values are not strongly dependent on temperature and are higher in Nafion® than in the composite membrane. The steric hindrance of crystallized water surrounding the filler and the side groups of Nafion® results in a reduced probability of proton hopping between active acid sites and consequently a decreased hopping distance.

In addition to the electrode polarization that is responsible for the long range conductivity of the composite membrane, two interfacial conductivity phenomena, σ_1 and σ_2, can be found at lower frequencies in both the dry and hydrated systems (refer to Figs. 6 and 7). These conductivities are due to the accumulation of charges along interfaces between domains that exhibit different characteristic permittivities.

The overall conductivity can be expressed as the summation of all of the conductivity phenomena as in Eq. (4) [49]:

$$\sigma_{\text{total}} = \sum_{i=0} \sigma_i = \sigma_0 + \sigma_1 + \sigma_2 \tag{4}$$

It is possible to consider that each conductivity contribution is the result of a different population of protons that have different characteristic frequencies and mobilities at any given temperature within the explored frequency range. In the dry membrane, the interfacial polarizations exist principally in the temperature region where σ_0 exhibits a VTF trend and therefore the conductivity is mediated by the motion of the host matrix. However unlike σ_0, σ_1 and σ_2 show Arrhenius behaviour, which indicates that these populations of protons move via a grothus-like "hopping" mechanism between proton-donor and acceptor sites along the interface between the hydrophilic and hydrophobic domains of the composite membrane. The presence of two different conduction mechanisms supports the interpretation that the interfacial

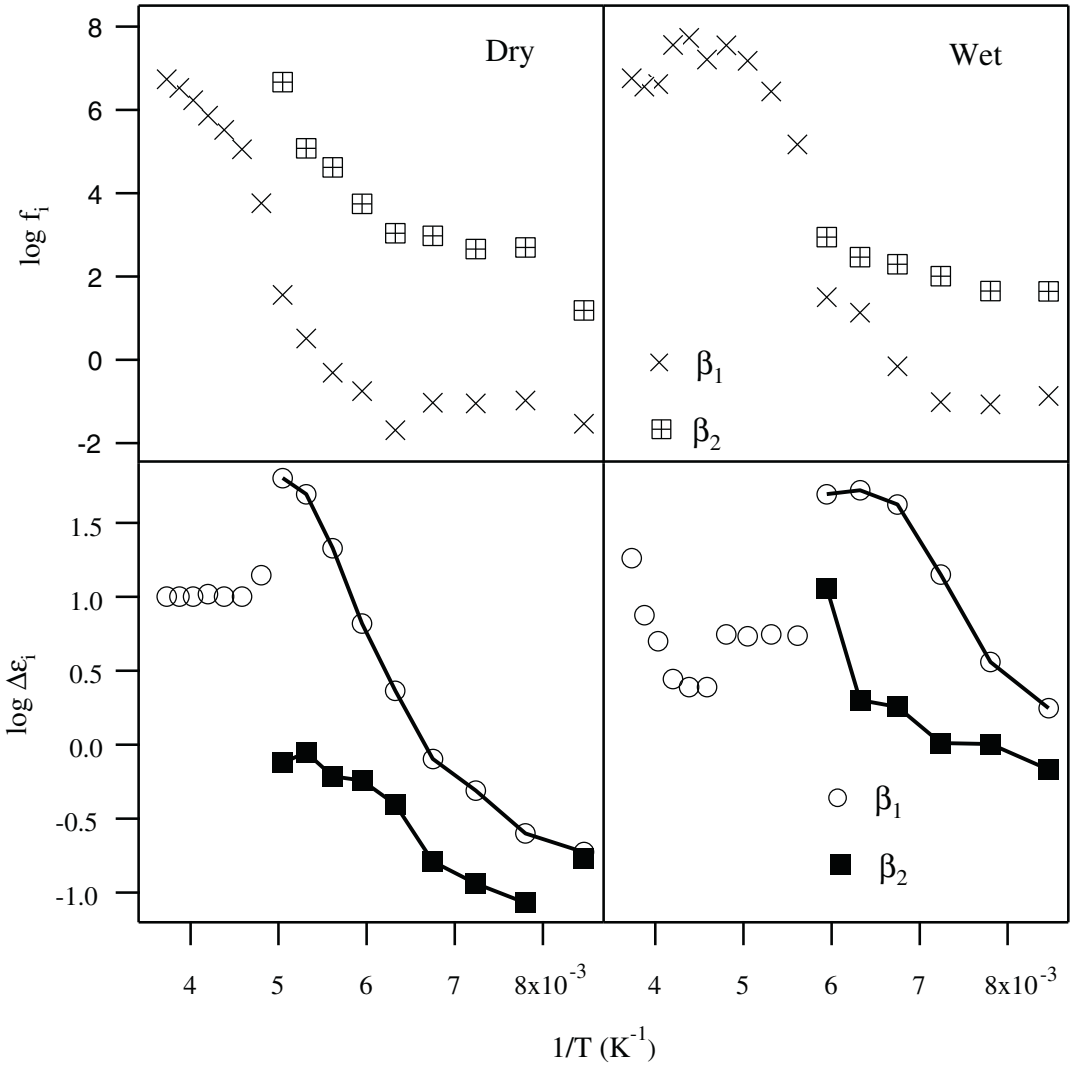

Fig. 12. Frequency and dielectric strength of β_1 and β_2 relaxations in dry and wet conditions.

conductivities are the result of different proton populations. The conductivity σ_1 can be divided into two temperature regions, one below 0 °C that has an activation energy of 66 ± 5 kJ mol^{-1} and another above 15 °C that has an activation equal to 96 ± 2 kJ mol^{-1}. The temperature dividing these regions corresponds to the α_1 transition. The large increase in activation energy is likely due to a decreased probability of an accessible proton site for the grothus-like mechanism resulting from the increased mobility of the polymer matrix. The conductivity σ_2 has an even higher activation energy, equal to 125 ± 2 kJ mol^{-1}. The conductivity values of these interfacial polarizations are at least two orders of magnitude lower than the conductivity σ_0. Therefore, the contribution of σ_1 and σ_2 to the overall long range conductivity, σ_{total}, are negligible and Eq. (4) is reduced to $\sigma_{total} = \sigma_0$.

The conductivities σ_1 and σ_2 of the fully hydrated membrane show Arrhenius-type behaviour. In the high and low temperature regions, respectively, σ_1 has activation energies equal to 62 ± 7 and 38 ± 3 kJ mol^{-1}, while σ_2 has an activation energy of 52 ± 4 kJ mol^{-1}. These activation energies are lower than those in the fully dehydrated conditions, which is likely the result of water facilitating the grothus-like conduction mechanism. It is interesting to note that at temperatures below but close to the melting point of water the values of conductivities σ_0 and σ_1 are within one order of magnitude. This indicates that in this temperature realm the interfacial conductivity makes a significant contribution to the long range conductivity. In addition, the activation energy of σ_1 below 0 °C is lower than the activation energy above 0 °C. As discussed above, solid water within the membrane decouples the motion of the backbone and the side chains in the host matrix. In this instance, the interface in a more immobile matrix provides a pathway for conduction. Above 0 °C, the contribution of σ_1 and σ_2 to the total conductivity can be considered negligible.

The dielectric strength and associated frequencies found from fitting the permittivity data with Eq. (1) are shown in Fig. 12 as a function of reciprocal temperature. The dielectric strength of β_1 and β_2 in the dry system increases with increasing temperature until −75 °C, at which point β_2 is no longer in the experimental frequency range and β_1 decreases slightly and then remains constant. The increase in dielectric strength is due to a decrease in the interaction strength associated with the side chain [42]. The decrease in β_1 and subsequent constant trend, which approximately corresponds to the β_2 transition, suggests that the dipoles of the two ether groups in the side chain are coupled and that the β_2 transition reduces the dielectric strength of β_1. The large increase in the frequency associated with β_1 at the β_2 transition supports this conclusion. Similar behaviour is seen in the fully hydrated membrane,

except an additional increase is seen in β_1 at −60 °C. This increase corresponds to the decrease in the interaction strength of the side chain up to and above the β_1 transition.

4. Conclusion

This study presents an interesting new type of composite membrane based on Nafion® doped with a sulfated-zirconia filler. This sulfated-zirconia filler is different from many others in that the filler itself can contribute to the proton conductivity due to the presence of acidic functionalities on the surface of the filler. The presence of the filler in the membrane results in the deprotonation of Nafion®'s acid moieties even in completely dry conditions as indicated by the absence of the acid mode at 1475 cm^{-1} in the FTIR spectrum. Spectra from DSC, DMA and BES show the presence of six molecular transitions: one γ, two β and three α. Only two of these molecular relaxations are detected in the BES permittivity profiles. None of the α transitions are found in the permittivity curves because they occur in the same temperature and frequency range as the polarizations. The polarizations have significantly larger permittivities making detection of the α relaxations impossible. The composite membrane exhibits a reasonably high conductivity (3×10^{-3} S cm^{-1}) even in completely dry conditions at 120 °C. The conductivity behaviour exhibits a mix of Arrhenius and VTF behaviours and is closely tied to the dielectric relaxations. At low temperatures, i.e. below the melting point of water, the conductivity of the wet membrane closely resembles that of the dry membrane and the long range conduction occurs via hopping-type mechanism. In the dry system at higher temperatures, the proton conduction mechanism is facilitated by the motion of the matrix. In the wet membrane above the melting point of water the long range conduction is largely driven by the water in the membrane, but to a small extent is mediated by the motion of the host matrix. The proton populations responsible for conduction along interfaces do not make a significant contribution to the long range conduction mechanism, except as the temperature approaches 0 °C in the wet membrane, where the interfaces provide a percolation pathway in polar domains that are sterically hindered by the presence of solid water.

Acknowledgements

This research was funded by the Italian MURST project PRIN2008, entitled "Direct polymer electrolyte membrane fuel cells: synthesis and study in prototype cells of hybrid inorganic–organic membranes and electrode materials". The authors extend their most sincere thanks to the staff of the mechanical workshop of the Department of Chemical Sciences of the University of Padova for the skillful technical assistance, particularly Mr. Stefano Mercanzin.

References

[1] G. Alberti, M. Casciola, Annu. Rev. Mater. Res. 33 (2003) 129–154.
[2] J.S. Wainright, M.H. Litt, R.F. Savinell, High-temperature membranes, in: W. Vielstich, A. Lamm, H.A. Gasteiger (Eds.), Handbook of Fuel Cells: Fundamentals Technology and Applications, Wiley, West Sussex, 2003, pp. 436–446.
[3] Y. Shao, G. Yin, Z. Wang, Y. Gao, J. Power Sources 167 (2007) 235–242.
[4] D.J. Jones, J. Rozière, Inorganic/organic composite membranes, in: W. Vielstich, A. Lamm, H.A. Gasteiger (Eds.), Handbook of Fuel Cells: Fundamentals Technology and Applications, Wiley, West Sussex, 2003, pp. 447–455.
[5] Q. Li, R. He, J.O. Jensen, N.J. Bjerrum, Chem. Mater. 15 (2003) 4896–4915.
[6] V. Di Noto, R. Gliubizzi, E. Negro, G. Pace, J. Phys. Chem. B 110 (2006) 24972–24986.
[7] V. Di Noto, S. Lavina, E. Negro, M. Vittadello, F. Conti, M. Piga, G. Pace, J. Power Sources 187 (2009) 57–66.
[8] V. Di Noto, E. Negro, J.Y. Sanchez, C. Iojoiu, J. Am. Chem. Soc. 132 (2010) 2183–2195.
[9] S.Y. Lee, A. Ogawa, M. Kanno, H. Nakamoto, T. Yasuda, M. Watanabe, J. Am. Chem. Soc. 132 (2010) 9764–9773.
[10] A. Martinelli, A. Matic, P. Jacobsson, L. Borjesson, A. Fernicola, S. Panero, B. Scrosati, H. Ohno, J. Phys. Chem. B 111 (2007) 12462–12467.
[11] M. Martinez, Y. Molmeret, L. Cointeaux, C. Iojoiu, J.C. Lepretre, N. El Kissi, P. Judeinstein, J.Y. Sanchez, J. Power Sources 195 (2010) 5829–5839.
[12] M. Nakao, M. Yoshitake, Composite perfluorinated membranes, in: W. Vielstich, A. Lamm, H.A. Gasteiger (Eds.), Handbook of Fuel Cells: Fundamentals Technology and Applications, Wiley, West Sussex, 2003, pp. 412–419.
[13] V. Di Noto, N. Boaretto, E. Negro, G.A. Giffin, S. Lavina, S. Polizzi, Int. J. Hydrogen Energy, in press, doi:10.1016/j.ijhydene.2011.07.132.
[14] V. Di Noto, N. Boaretto, E. Negro, P.E. Stallworth, S. Lavina, G.A. Giffin, S.G. Greenbaum, Int. J. Hydrogen Energy, in press, doi:10.1016/j.ijhydene.2011.07.135.
[15] V. Di Noto, R. Gliubizzi, E. Negro, M. Vittadello, G. Pace, Electrochim. Acta 53 (2007) 1618–1627.
[16] V. Di Noto, M. Piga, S. Lavina, E. Negro, K. Yoshida, R. Ito, T. Furukawa, Electrochim. Acta 55 (2010) 1431–1444.
[17] V. Di Noto, M. Piga, L. Piga, S. Polizzi, E. Negro, J. Power Sources 178 (2008) 561–574.
[18] M.A. Navarra, C. Abbati, F. Croce, B. Scrosati, Fuel Cells 9 (2009) 222–225.
[19] M.A. Navarra, C. Abbati, B. Scrosati, J. Power Sources 183 (2008) 109–113.
[20] S. Tominaka, N. Akiyama, F. Croce, T. Momma, B. Scrosati, T. Osaka, J. Power Sources 185 (2008) 656–663.
[21] S. Tominaka, T. Momma, B. Scrosati, T. Osaka, J. Power Sources 195 (2010) 4065–4071.
[22] M.A. Navarra, F. Croce, B. Scrosati, J. Mater. Chem. 17 (2007) 3210–3215.
[23] S. Hara, M. Miyayama, Solid State Ionics 168 (2004) 111–116.
[24] M. Amirinejad, S.S. Madaeni, M.A. Navarra, E. Rafiee, B. Scrosati, J. Power Sources 196 (2011) 988–998.
[25] G.M. Haugen, F. Meng, N.V. Aieta, J.L. Horan, M.-C. Kuo, M.H. Frey, S.J. Hamrock, A.M. Herring, Electrochem. Solid-State Lett. 10 (2007) B51–B55.
[26] J.L. Horan, J.A. Turner, A.M. Herring, S.F. Dec, Prepr. Symp. – Am. Chem. Soc., Div. Fuel Chem. 51 (2006) 653–655.
[27] Z. Chen, B. Holmberg, W. Li, X. Wang, W. Deng, R. Munoz, Y. Yan, Chem. Mater. 18 (2006) 5669–5675.
[28] B.A. Holmberg, X. Wang, Y. Yan, J. Membr. Sci. 320 (2008) 86–92.
[29] B. Decker, C. Hartmann-Thompson, P.I. Carver, S.E. Keinath, P.R. Santurri, Chem. Mater. 22 (2010) 942–948.
[30] S. Subianto, M.K. Mistry, N.R. Choudhury, N.K. Dutta, R. Knott, ACS Appl. Mater. Interfaces 1 (2009) 1173–1182.
[31] A. D'Epifanio, M.A. Navarra, F.C. Weise, B. Mecheri, J. Farrington, S. Licoccia, S. Greenbaum, Chem. Mater. 22 (2010) 813–821.
[32] M.K. Mishra, B. Tyagi, R.V. Jasra, Ind. Eng. Chem. Res. 42 (2003) 5727–5736.
[33] M. Vittadello, E. Negro, S. Lavina, G. Pace, A. Safari, V. Di Noto, J. Phys. Chem. B 112 (2008) 16590–16600.
[34] V. Bolis, G. Magnacca, G. Cerrato, C. Morterra, Langmuir 13 (1997) 888–894.
[35] C. Morterra, G. Cerrato, F. Pinna, M. Signoretto, J. Phys. Chem. 98 (1994) 12373–12381.
[36] V. Di Noto, M. Piga, G. Pace, E. Negro, S. Lavina, ECS Trans. 16 (2008) 1183–1193.
[37] L.K.H. Beek, J.B. Birks (Eds.), Progress in Dielectrics, Heywood, London, 1967.
[38] I.M. Hodge, A. Eisenberg, Macromolecules 11 (1978) 289–293.
[39] F. Kremer, A. Schoenhals, Broadband Dielectric Spectroscopy, Springer-Verlag, Berlin, 2003.
[40] K.A. Page, K.M. Cable, R.B. Moore, Macromolecules 38 (2005) 6472–6484.
[41] V. Di Noto, J. Phys. Chem. B 106 (2002) 11139–11154.
[42] V. Di Noto, G.A. Giffin, K. Vezzù, M. Piga, S. Lavina, Broadband dielectric spectroscopy: a powerful tool for the determination of charge transfer mechanisms in ion conductors, in: P. Knauth, M.L. Di Vona (Eds.), Solid State Proton Conductors: Properties and Applications in Fuel Cells, Wiley, Chichester, 2012.
[43] V. Di Noto, E. Negro, S. Lavina, M. Vittadello, Hybrid inorganic–organic polymer electrolytes, in: C. Sequeira, D. Santos (Eds.), Polymer Electrolytes – Fundamentals and Applications, Woodhead Publishing Limited, Oxford, 2010, pp. 219–277.
[44] V. Di Noto, M. Vittadello, S.G. Greenbaum, S. Suarez, K. Kano, T. Furukawa, J. Phys. Chem. B 108 (2004) 18832–18844.
[45] M. Vittadello, S. Suarez, S.H. Chung, K. Fujimoto, V. Di Noto, S.G. Greenbaum, T. Furukawa, Electrochim. Acta 48 (2003) 2227–2237.
[46] P. Atkins, J. de Paula, Physical Chemistry, 8th ed., Oxford University Press, Oxford, 2006.
[47] K.D. Kreuer, J. Membr. Sci. 185 (2001) 29–39.
[48] K.J. Oberbroeckling, D.C. Dunwoody, S.D. Minteer, J. Leddy, Anal. Chem. 74 (2002) 4794–4799.
[49] V. Di Noto, M. Piga, G.A. Giffin, S. Lavina, E.S. Smotkin, Jean-Yves, Sanchez, C. Iojoiu, J. Phys. Chem. C, submitted for publication.